Topologically Protected Vortex flows in High Voltage AC Power Grids: Supplemental Material

T. Coletta,[1] R. Delabays,[1,2] I. Adagideli,[3] and Ph. Jacquod[1]

[1] *School of Engineering, University of Applied Sciences of Western Switzerland, CH-1950 Sion, Switzerland*

[2] *Section de Mathématiques, Université de Genève, CH-1211 Genève, Switzerland*

[3] *Faculty of Engineering and Natural Sciences, Sabanci University, Orhanli-Tuzla, Istanbul, Turkey*

(Dated: August 12, 2016)

S1. THE POWER FLOW PROBLEM

Power grids are AC electrical networks. Mathematically speaking, they are modeled as graphs with n nodes, each of them representing a bus and the graph's edges representing electrical lines.

The standard operating state of electric power grids is characterized by synchrony, where voltage angles on all buses rotate at the same frequency. That state is reached and maintained thanks to the coupling between buses induced by power lines and a balance regulation between power production and consumption, which forbid voltage angles from deviating from a predetermined frequency by more than a fraction of a percent. Production and consumption are constantly fluctuating and accordingly the synchronous state of the system constantly changes. Most of the time, however, these changes are so slow that the whole system is effectively in a steady-state determined by one of the solutions to the *power flow equations*,

$$P_l = \sum_m B_{lm}\,|V_l||V_m|\,\sin(\theta_l-\theta_m) + G_{lm}\left[|V_l|^2 - |V_l||V_m|\cos(\theta_l-\theta_m)\right]\,, \tag{S1a}$$

$$Q_l = \sum_m B_{lm}\,\left[|V_l|^2 - |V_l||V_m|\cos(\theta_l-\theta_m)\right] - G_{lm}\,|V_l||V_m|\,\sin(\theta_l-\theta_m)\,, \tag{S1b}$$

which we take as our starting point. These are transcendental equations for balanced 3-phase systems [1], which relate the phase and amplitude of the complex AC voltage $V_m = |V_m|\exp[i\theta_m]$ at the bus connecting the m^{th} component (a producer or a consumer) to the grid, to the active, P_l, and reactive, Q_l, powers injected ($P_l, Q_l > 0$) or consumed ($P_l, Q_l < 0$) at the l^{th} bus via power lines of complex admittance $Y_{lm} = G_{lm} + iB_{lm}$. In its full version, the problem is defined by splitting the n buses into producer and consumer buses with pre-determined $\{P_l, |V_l|\}$ and $\{P_l, Q_l\}$ respectively. With these conditions fixed, Eqs. (S1) then determine angles at all buses, voltages at consumer buses and reactive powers at producer buses.

High voltage power lines typically have a conductance to susceptance ratio $G_{lm}/B_{lm} < 0.1$, becoming smaller at higher voltage. A first level of approximation is thus to neglect the conductance and with it all ohmic dissipation and to consider

$$P_l = \sum_m B_{lm}|V_l||V_m|\,\sin(\theta_l-\theta_m)\,, \tag{S2a}$$

$$Q_l = \sum_m B_{lm}\,\left[|V_l|^2 - |V_l||V_m|\cos(\theta_l-\theta_m)\right]\,. \tag{S2b}$$

Eqs. (S2) give the lossless line approximation. At that level, one may consider voltage variations that are necessary to accomodate predetermined amounts of reactive power Q_l at consumer nodes.

However, a standardly used level of approximation [2–4] is to neglect voltage variations and consider $|V_l| = V_0$, $\forall l$, to introduce an effective line susceptance $\tilde{B}_{lm} = B_{lm}V_0^2$, and to focus on the power flow equation for the active power only, Eq. (S2a), since, within that approximation, it decouples from the reactive power. We will follow that approach. Within the lossless line approximation, the analogy between AC power grids and current biased Josephson junction arrays is evident : power flows between buses l and m in AC power grids have the same sinusoidal dependence on voltage angle differences, $\tilde{B}_{lm}\sin(\theta_l - \theta_m)$, that Josephson currents between two tunnel-coupled superconductors have on the phases of the order parameters [5].

The fact that the lines are lossless manifests itself in the power balance between production and consumption, $\sum_l P_l = 0$. When the conductance G_{lm} is not negligible, the power dissipated must be compensated by an increased power injection. When dissipation is taken into account, one has

$$\sum_l P_l = \sum_{l,m} \tilde{G}_{lm}\ [1 - \cos(\theta_l - \theta_m)]\ , \tag{S3}$$

where we defined $\tilde{G}_{lm} \equiv G_{lm}V_0^2$. Starting from the lossless perspective and considering dissipative effects as a perturbation, it is evident from Eq. (S3) that different solutions to Eq. (S2a) dissipate different amounts of power. Thus, for the full problem (including dissipation), these different solutions generally require different power injections and the power flow problem is no longer defined a priori by a set of power injections $\{P_i\}$ which sum up to zero. Power production must be greater than the consumption to compensate the ohmic losses. Thus power injection must be adapted self-consistently with the angles. In our simulations we will achieve that by increasing/decreasing power injection depending on the frequency of the synchronous solution as obtained from the swing equations, Eq. (S12). This procedure is iterated until the dynamical system converges toward a synchronous stationary solution having the reference frequency. Clearly ohmic losses can be compensated by different injection profiles and this procedure is a priori not uniquely defined. A standard procedure in electrical engineering is to predetermine all but one power injections and consumptions and introduce a *slack bus*, that injects whatever additional power is needed to balance production with consumption and satisfy Eq. (S3). This is the approach we follow in our simulations on simple network topologies presented hereafter and in the main text. For the simulation of the complex network having the topology of the UK transmission grid (see main text) we assume instead that all producers equally compensate for the ohmic losses.

S2. NUMBER OF DIFFERENT POWER FLOW SOLUTIONS

Refs. [6, 7] showed that different solutions to the dissipationless power flow Eq. (S2) exist on meshed networks, and that these different solutions are related to one another by circulating loop flows, i.e. power flows going around closed loops formed in the network. We sketch here the proof of that theorem. It is based on the *incidence matrix* A of the network, whose row indices correspond to nodes (buses) and column indices to the network edges (the links between nodes), and which is defined as

$$A_{li} = \begin{cases} 1\,, & \text{if node } l \text{ is the source of edge } i\,, \\ -1 & \text{if node } l \text{ is the target of edge } i\,, \\ 0\,, & \text{otherwise}\,. \end{cases} \tag{S4}$$

The dissipationless power flow problem can be rewritten in terms of the incidence matrix as

$$P_l = \sum_i A_{li}\, I_i\,, \tag{S5}$$

where I_i is a component of the vector of flows on the network's edges. It is easy to see that two solutions of Eq. (S5) differ by a flow vector with components δI_i satisfying

$$0 = \sum_i A_{li}\, \delta I_i\,, \tag{S6}$$

and which therefore belongs to the kernel of the incidence matrix. The proof is completed by invoking a known result of algebraic graph theory that any element in $\ker(A)$ is a linear combination of unitary flows along loops formed in the network [8]. Reference [7] also discusses how these different solutions can be labeled by integer topological winding numbers.

We qualitatively discuss the fate of circulating loop flows in cases with dissipation, i.e. nonegligible conductance. From Eq. (S4), for each element of the incidence matrix $A_{li} \neq 0$ there is exactly one $A_{mi} = -A_{li}$, where l and m label the two ends of edge i. Thus contributions from each nondissipative, susceptive flow I_i appear for both ends of edge i in Eq. (S5), contributing to P_l and P_m with opposite sign. This parity antisymmetry is characteristic of nondissipative flows. On the contrary, the dissipative part of the flow is parity symmetric - a current of fixed magnitude on a given edge gives the same dissipation, regardless of the direction in which it traverses the line. Adding dissipation therefore requires to add a *resistance* matrix R with $R_{li} = |A_{li}|$. Eq. (S5) becomes, in the presence of dissipation

$$P_l = \sum_i A_{li}\, I_i + R_{li}\, J_i\,, \tag{S7}$$

with a dissipated power flow $J_i \geq 0$. The difference between two power flow solutions then reads

$$\delta P_l = \sum_i A_{li}\, \delta I_i + R_{li}\, \delta J_i \,. \tag{S8}$$

Summing over all nodes one gets

$$\sum_l \delta P_l = \sum_{l,i} R_{li}\, \delta J_i \,, \tag{S9}$$

which, similarly as Eq. (S3), says that the net total injected power is solely due to the dissipative part of the power flow. Assuming that the equality in Eq. (S9) holds term by term, one obtains again Eq. (S6) so that the two solutions differ by loop flows only. How this can be achieved in practice is easily seen starting from the lossless line approximation, Eq. (S2), which, as was shown in Refs. [6, 7], carries solutions $\{\theta_i^{(0)}\}$ differing by loop flows only. Once dissipation is added, these solutions remain valid if one chooses to change the injected and consumed powers as $P_l \to P_l + \delta P_l$ with

$$\delta P_l = \sum_m \bar{G}_{lm} \left[1 - \cos(\theta_l^{(0)} - \theta_m^{(0)})\right] \,. \tag{S10}$$

This suggests that, at least for not too strong dissipation, i.e. for weak conductance to susceptance ratios, different solutions to the power flow problem exist. For two such solutions, the transmitted powers still differ by loop flows. Extending the results of Refs. [6, 7] is straightforward with the choice of Eq. (S10) for compensating losses, because angles are not modified. In the main text, we numerically use another procedure, where the additional power necessary to counterbalance ohmic losses is injected from a single bus. This is a standard approach in electrical engineering where a *slack bus* ensures that the total power balance is satisfied [1].

Because the power flow problem in the presence of dissipation becomes higher-dimensional, with additional degrees of freedom related to the choice of producers in charge of compensating the ohmic dissipation, it is much harder to make general statements about the extension of the theorem of Refs. [6, 7] to that case. Nevertheless, from Eq. (S10) it is clear that since solutions indexed by high topological winding numbers (i.e. solutions carrying large loop flows) are characterized by larger phase differences, they will in general lose more power to ohmic losses.

S3. DYNAMICS AND STABILITY

For each producer and consumer bus, energy conservation states that the injected or consumed power is equal to the transmitted power (with a negative or positive sign depending on whether it

flows toward or away from the bus considered) minus the losses, including transmission line losses as well as mechanical damping losses. This balance condition leads to the *swing equations* [1]

$$M_l\ddot{\theta}_l + \dot{\theta}_l = P_l - \sum_m \left(B_{lm}\,|V_l||V_m|\,\sin(\theta_l - \theta_m) + G_{lm}\left[|V_l|^2 - |V_l||V_m|\cos(\theta_l - \theta_m)\right]\right)\,, \qquad \text{(S11)}$$

which we write here in a frame rotating with the frequency $\Omega/2\pi = 50$ or 60 Hz of the grid. The terms $M_l\ddot{\theta}_l$ and $\dot{\theta}_l$ in Eq. (S11) represent the change in rotational kinetic energy and the damping of the rotating machines connected to the grid.

In this work we consider a simplified version of the swing equations where the mechanical inertia of generators is neglected, i.e. where instead of Eq. (S11) we consider

$$\dot{\theta}_l = P_l - \sum_m \tilde{B}_{lm}\,\sin(\theta_l - \theta_m) + \tilde{G}_{lm}\,[1 - \cos(\theta_l - \theta_m)]\,. \qquad \text{(S12)}$$

While the inertia term affects stability time scales [1], it does not influence whether a solution is linearly stable or not, which is our interest here. In particular it can be shown that linear stability is lost for a power grid modeled by Eq. (S12) at the same time it would be lost for the same set of equations extended with inertia terms with any distribution of inertia $\{M_l\}$ [9, 10]. We therefore neglect inertia terms from now on.

Solutions to the power flow equations, Eq. (S1), are stationary solutions of the swing equations, Eq. (S12). The latter allows to determine the linear stability of power flow solutions $\{\theta_l^{(0)}\}$ under small perturbations, $\theta_l^{(0)} \to \theta_l^{(0)} + \delta\theta_l$. Within the lossless line approximation, the linearized dynamics reads

$$\delta\dot{\theta}_l = -\sum_m \tilde{B}_{lm}\,\cos(\theta_l^{(0)} - \theta_m^{(0)})(\delta\theta_l - \delta\theta_m)\,. \qquad \text{(S13)}$$

The linear stability of the solution is therefore determined by the spectrum of the *stability matrix* $M(\{\theta_l^{(0)}\})$,

$$M_{lm} = \begin{cases} \tilde{B}_{lm}\cos(\theta_l^{(0)} - \theta_m^{(0)}) & \text{if } l \neq m\,, \\ -\sum_{k\neq l} \tilde{B}_{lk}\cos(\theta_l^{(0)} - \theta_k^{(0)}) & \text{if } l = m\,, \end{cases} \qquad \text{(S14)}$$

which depends on the angles at the stationary, phase-locked solution. The eigenvalues of M are the so-called Lyapunov exponents [11]. Without dissipation, M is real symmetric, therefore all Lyapunov exponents are real, furthermore one of them always vanishes, $\lambda_1 = 0$, because $\sum_j M_{ji} = \sum_j M_{ij} = 0$. This condition is similar to a gauge invariance according to which only angle differences matter. The stationary state is thus linearly stable if M is negative semidefinite and unstable otherwise. Equivalently, stability is ensured as long as the largest nonvanishing eigenvalue λ_2 of M remains negative.

In the dissipative case, the definition of the stability matrix generalizes to

$$M_{lm} = \begin{cases} \tilde{B}_{lm}\cos(\theta_l^{(0)} - \theta_m^{(0)}) - \bar{G}_{lm}\sin(\theta_l^{(0)} - \theta_m^{(0)}) & \text{if } l \neq m\,, \\ -\sum_{k\neq l}\left(\tilde{B}_{lk}\cos(\theta_l^{(0)} - \theta_k^{(0)}) - \bar{G}_{lk}\sin(\theta_l^{(0)} - \theta_k^{(0)})\right) & \text{if } l = m\,. \end{cases} \tag{S15}$$

Thus, in the presence of dissipation, the stability matrix maintains its zero row sum property (ensuring that $\lambda_1 = 0$) but is no longer symmetric which can lead to a complex spectrum. In this case linear stability is ensured as long as the real part of all nonvanishing eigenvalues of M is negative. To make contact with the nondissipative case, we denote by λ_2 the eigenvalue having the largest real part.

S4. DYNAMICAL GENERATION OF VORTICES

The first mechanism for generating vortex flows discussed in the main text is based on the loss of stability of power flow solutions with lower winding numbers while solutions with higher winding numbers remain stable. This is done by increasing power generated and consumed, which, depending on the grid's geometry leads to a line congestion and a temporary dynamical instability, eventually driving the system to a new, stable stationary state with redistributed power flows. The model considered in the main text is a ring of $n = 18$ nodes, with one main producer at node 1 and one main consumer at node 7. Small random injections at all other nodes are introduced to remove a mirror symmetry along the axis going through nodes 4 and 13. This symmetry results in $\dot{\theta}_i = -\dot{\theta}_{\mathcal{P}(i)}$ with $\mathcal{P}(i)$ denoting the mirror symmetric node to i. Analytically, this forbids transitions to other q-values starting from any stationary $q = 0$ states. Numerically it results in very long transients with anomalously long angle rotations. To show that our model is generic and that its behavior is not an artefact of random injections/consumptions we discuss a different model which corroborates our conclusions in the main text.

In Fig. S1 we illustrate a similar mechanism based on the weakening of a line on a network loop by an additional power injection. We consider a single loop of $n = 12$ nodes and lines of capacity B_0. Initially, a first producer supplies $P_1 = B_0$ units of power to a consumer located four nodes away from it. The transmitted power splits over the two possible paths joining the producer to the consumer. Next, the consumption is increased from $-P_1$ to $-P_1 - P_2$. To meet this additional power demand, a second generator, neighboring the consumer, injects a power $P_2 > 0$ (see inset of Fig. S1). This additional power injection increases the load of the line connecting the consumer to the second generator. This weakening of the transmission path eventually drives part of the

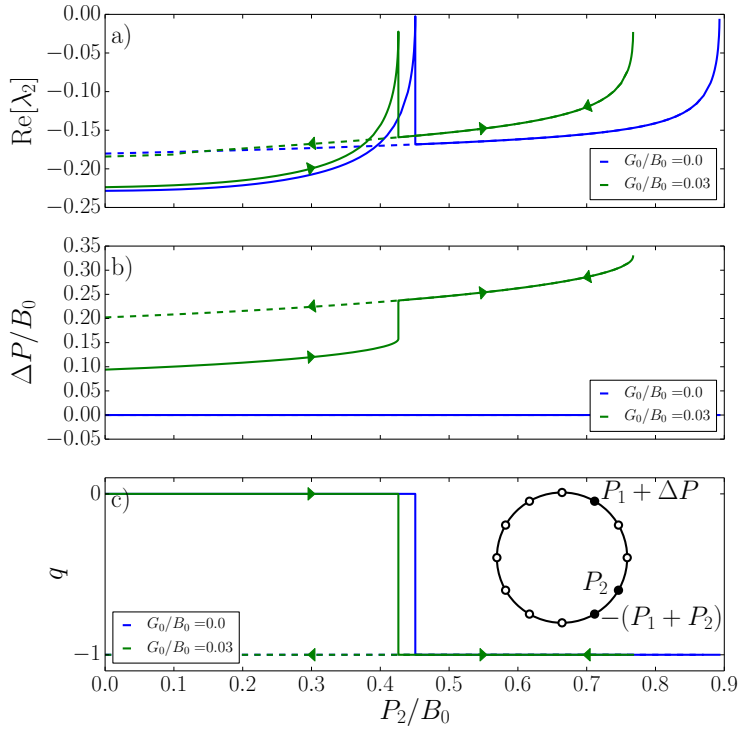

FIG. S1. Dynamical generation of vortices by line weakening for a ring with $n = 12$ nodes and lines of susceptance B_0. Locations of the main power injections and consumptions are indicated by the black nodes in the inset of panel c), while all white nodes have small random injections and consumptions summing to zero, to make the model more generic. As the consumer demand is increased from $-P_1 = -B_0$ to $-P_1 - P_2$ units of power, the transmission path connecting the comsumer to its neighboring producer weakens forcing additional power to flow around the other side of the loop. As the power demand is increased beyond $P_2 \simeq 0.45B_0$ for the lossless case, and $P_2 \simeq 0.42B_0$ for the dissipative case $G_0/B_0 = 0.03$, the $q = 0$ solution becomes unstable [panel a)] driving the system into a state with winding number $q = -1$. This state is highly dissipative and, as indicated by the arrows, it is topologically protected.

injection of the first producer away from its original path, around the other side of the loop. Fig. S1 illustrates this mechanism respectively in the lossless and dissipative cases where, for the latter, the first generator is in charge of fully compensating the ohmic losses ΔP. The $q = 0$ solution loses stability when the additional power injection reaches $P_2 \simeq 0.45B_0$ (resp. $P_2 \simeq 0.42B_0$ for $G_0/B_0 = 0.03$), which drives the system to the $q = -1$ solution. That solution remains stable until $P_2 \simeq 0.9B_0$ (resp. $P_2 \simeq 0.77B_0$ for $G_0/B_0 = 0.03$). In the dissipative case, the $q = -1$ solution significantly increases ohmic losses doubling them at $P_2 = 0$. The arrows indicate the hysteretic behavior where decreasing P_2 from the $q = -1$ solution at $P_2 \simeq 0.77B_0$ does not bring the system back to the $q = 0$ solution. This topological protection forces the power system to produce more

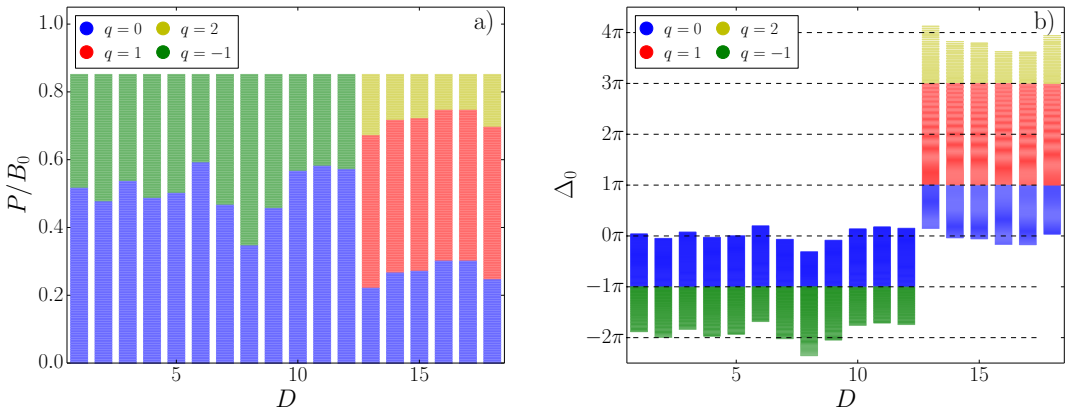

FIG. S2. Vortex generation under the line reclosure mechanism, for the single-loop model shown in the inset of Fig. 1d in the main text, with additional random power injection in the intermediate nodes. The final winding numbers, after reclosure, are color-coded and plotted as a function of the position D of the tripped line and a) the rescaled injected power P/B_0, b) the angle differences Δ_0 between the two ends of the tripped line. Vortex generation occurs as soon as $\Delta_0 \geq \pi$ and higher winding numbers q are reached each time Δ_0 crosses an odd integer multiple of π. This shows that the argument presented in the main text holds even in the more general situation with power injections between the main producer and the main consumer.

to compensate for the additional ohmic losses despite the existence of a less dissipative solution. When the system is in the $q = -1$ state for $P_2 \lesssim 0.42B_0$, reducing ΔP to the value required by the $q = 0$ solution drives the system to a $q = -1$ synchronous state with reduced frequency, but not to the $q = 0$ state.

S5. GENERATION OF VORTICES BY LINE RECLOSURE

The line reclosure mechanism discussed in the main text considers a big producer connected to a big consumer on a loop where all other buses have $P_l = 0$. This allows to project the $(n-1)$-dimensional configuration space of angles on a two-dimensional space and in this way to visualize the basins of attraction of solutions with different winding numbers (Fig. 2c and d of the main text). It was found that the winding numbers change by one each time the angle difference Δ_0 between the buses at the two ends of the line to be reclosed crosses an odd integer multiple of π. These findings are generic, in that they remain valid under the addition of randomly distributed power injections/consumptions on intermediate buses between the big producer and consumer. This is illustrated in Fig. S2. Compared to Fig. 2 of the main text, the presence of

random injections/consumptions strongly modifies the borders between reconnected solutions with different q in the P/B vs. D plane (panel a) but not in the Δ_0 vs. D plane (panel b). This is so because the small random injections change the value of P necessary for $\Delta_0 = (2p+1)\pi$. One sees that, despite the presence of random power injections, vortex flows are generated by line reconnection as soon as $|\Delta_0| > \pi$, but not earlier, and that the created vortex has a winding number increasing/decreasing as $\Delta q = \mathrm{mod}(\Delta_0 + \pi, 2\pi)$ with good precision. This confirms that the findings presented in the main text are generic and not restricted to the a priori ideal situation considered there.

S6. BASINS OF ATTRACTION AND THE PROJECTED LYAPUNOV FUNCTION

In this section we present some details on the projection of the Lyapunov function and on the basins of attraction of solutions having different winding numbers in the context of the line tripping and reclosure mechanism for the model depicted in the inset of Fig. 1d of the main text.

In the main text, we show that the Lyapunov function projected on the $(\Delta_\mathrm{L}, \Delta_\mathrm{R})$-plane reads,

$$\begin{aligned}\mathcal{V}(\Delta_\mathrm{L}, \Delta_\mathrm{R}) &= -N_\mathrm{L} P \Delta_\mathrm{L} - N_\mathrm{L} B_0 \cos\Delta_\mathrm{L} - (N_\mathrm{R}-1) B_0 \cos\Delta_\mathrm{R} - B_0 \cos(\Delta_0) \\ &= -N_\mathrm{L} P \Delta_\mathrm{L} - N_\mathrm{L} B_0 \cos\Delta_\mathrm{L} - (N_\mathrm{R}-1) B_0 \cos\Delta_\mathrm{R} - B_0 \cos(N_\mathrm{L}\Delta_\mathrm{L} - (N_\mathrm{R}-1)\Delta_\mathrm{R})\,.\end{aligned} \tag{S16}$$

This is Eq. (9) in the main text. Also in the main text, we show that the point $(\Delta_\mathrm{L}, \Delta_\mathrm{R}) = (\arcsin(P/B_0), 0)$ (the system's state just before reclosure of the faulty line) is a saddle of the Lyapunov function (S16), if P is such that $N_\mathrm{L}\Delta_\mathrm{L} = (2p+1)\pi$ for $p \in \mathbb{Z}$. Inspection of the Hessian of the Lyapunov function allows us further to show that $(\Delta_\mathrm{L}, \Delta_\mathrm{R}) = (\arcsin(P/B_0), 0)$ for $N_\mathrm{L} \arcsin(P/B_0) = (2p+1)\pi$ is a saddle point of the projected Lyapunov function. Fig. S3 gives a contour plot of the Lyapunov function for the 18 node cycle network considered in the main text. Depending on the value of the power injected [panels a) to c)], the state of the system at the moment of the line reclosure lies either in the basin of attraction of the $q = 0$ solution, or in that of the $q = 1$ solution, or at a saddle point separating them.

[1] A. R. Bergen and V. Vittal, *Power Systems Analysis* (Prentice Hall, 2000).

[2] G. Filatrella, A. H. Nielsen, and N. F. Pedersen, The European Physical Journal B **61**, 485 (2008).

[3] N. Chopra and M. W. Spong, IEEE Transactions on Automatic Control **54**, 353 (2009).

[4] A. Arenas, A. Díaz-Guilera, J. Kurths, Y. Moreno, and C. Zhou, Physics Reports **469**, 93 (2008).

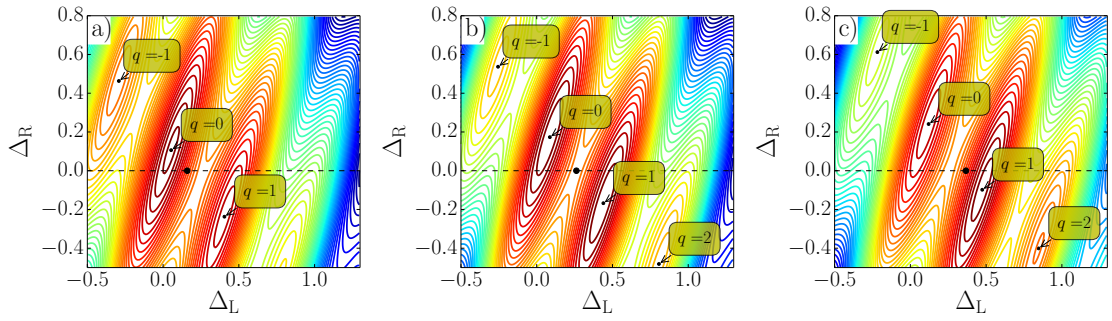

FIG. S3. Contour plots of the projected Lyapunov function for the 18 node cycle network described in the main text [see Fig. 1d)] and injected powers $P \approx 0.159B_0$ panel a), $P = B_0 \sin(\pi/12) \approx 0.259B_0$ panel b), and $P \approx 0.359B_0$ panel c). Local minima at different values of q are indicated. The operating state obtained by tripping one line on the shortest path between the generator and the producer ($\Delta_R = 0$, $\Delta_L = \arcsin(P/B_0)$, and $\Delta_0 = 12\Delta_L$) is indicated by the black dot on each panel. It lies in the basin of attraction of the $q = 0$ state for $P < 0.259B_0$ [case a)], in the basin of atttraction of the $q = 1$ state for $P > 0.259B_0$ [case c)], and at the saddle point separating the two basins for $P = 0.259B_0$ [case b)].

[5] B. D. Josephson, Phys. Lett. **1**, 251 (1962).

[6] F. Dörfler, M. Chertkov, and F. Bullo, Proc. Natl. Acad. Sci. **110**, 2005 (2013).

[7] R. Delabays, T. Coletta, and P. Jacquod, J. Math. Phys. **57**, 032701 (2016).

[8] N. Biggs, *Algebraic graph theory*, 2nd ed. (Cambridge University Press, 1993).

[9] T. Coletta and P. Jacquod, Phys. Rev. E **93**, 032222 (2016).

[10] D. Manik, D. Witthaut, B. Schäfer, M. Matthiae, A. Sorge, M. Rohden, E. Katifori, and M. Timme, Eur. Phys. J. Special Topics **223**, 2527 (2014).

[11] M. A. Pai, *Energy Function Analysis for Power System Stability* (Kluwer Academic Publishers, 1989).